Molecular simulation and theory of a liquid crystalline disclination core

Denis Andrienko and Michael P. Allen
H. H. Wills Physics Laboratory, University of Bristol, Royal Fort, Tyndall Avenue, Bristol BS8 1TL, United Kingdom
(Received 9 July 1999; revised manuscript received 7 September 1999)

Molecular simulations of a nematic liquid crystal confined in cylinder geometry with homeotropic anchoring have been carried out. The core structure of a disclination line defect of strength +1 has been examined, and comparison made with various theoretical treatments, which are presented in a unified way. It is found that excellent fits to the cylindrically symmetrized order tensor profiles may be obtained with appropriate parameter choices; notwithstanding this, on the time scales of the simulation, the cylindrical symmetry of the core is broken and two defects of strength $+\frac{1}{2}$ may be resolved.

PACS number(s): 61.30.Cz, 61.30.Jf, 61.20.Ja, 07.05.Tp

I. INTRODUCTION

Liquid crystals are at the heart of a range of technological devices that rely on the ability to manipulate the direction of preferred molecular alignment, the *director* **n**, with electric and magnetic fields, and through coupling to surfaces. The practical performance of such devices and the theoretical description of director distortions both rely on smooth variation of the director with position in space; this is well accounted for by the Frank free energy [1,2], which is an expansion in squared gradients of the director field $\mathbf{n}(\mathbf{r})$, parametrized by the splay (K_{11}), twist (K_{22}), and bend (K_{33}) elastic constants. The director **n** is the principal axis of the local second-rank ordering tensor **Q**, which characterizes the nematic state; such a description is intrinsically uniaxial and neglects variation of the *degree* of ordering with position, of the kind that occurs near bounding surfaces and around topological defects. Such defects are treated as singularities in the director field; for a better description, it is necessary to replace the director field with one that allows some variation of the relevant order tensor components over relatively short length scales. The relevant region near the defect is called the *core*.

The most common type of defect in the nematic phase is the disclination line defect, characterized by an integer or half-integer index defined by the number of turns of the director field associated with taking a circuit about the line. The phenomenological approach to the investigation of line defects was described by Schopohl and Sluckin [3,4]. They worked with the full order-parameter tensor $Q_{\alpha\beta}$ in the framework of Landau–de Gennes theory, and applied this to the structure of the $\pm\frac{1}{2}$ disclination core. The *full* order parameter $Q_{\alpha\beta}$ was used (a) to avoid *divergent* terms in the elastic energy and (b) to take into account possible *biaxiality* of the defect core. Then the general idea was implemented for the particular problem of the core structure of the ±1 strength defect: Biscari and Virga [5] and Mottram and Hogan [6] solved the equations for the order tensor and obtained order parameter and biaxiality profiles. They used truncated expansions of the free-energy density, which helped them to obtain analytical solutions to the problem. Finally, Sigillo *et al.* [7] considered the +1 disclination problem in the spirit of Maier-Saupe mean-field theory.

In this paper we use the approach proposed by Schopohl and Sluckin to obtain the order parameter profiles near the disclination line. We also recapitulate the results of the other theories in order to discuss the advantages and disadvantages of the proposed models. We compare these predictions with the results of computer simulation using a simple molecular model. Computer simulation is a well established method of relating bulk elastic coefficients [8–14], and more recently surface anchoring strengths [15,16], to molecular structure and interaction parameters. An early study of disclination line defects [17] involved Monte Carlo simulations of rodlike molecules (hard spherocylinders) confined in cylindrical geometry with boundary conditions chosen to stabilize the chosen director field far from the defect. This work concentrated on the disclination line defect of strength $-\frac{1}{2}$, in cylinders of radius 2–3 times the molecular length. For short rods, smooth variation of the order parameters with position was observed, and the defect core retained axial symmetry. For longer rods, having much larger bend elastic constants, this symmetry was broken, and various microscopically ''escaped'' structures were seen. There was also evidence of metastability, and nonconvergence of structures from different starting configurations, which the authors attempted to resolve using free-energy calculations. More recently, a study of two-dimensional models has been carried out [18]. These studies support the view that the disclination core is one or two molecular lengths across.

The purpose of this paper is to present simulation results for a model of hard particles in a cylindrical pore, following closely the approach of Ref. [17], and compare with the theories just mentioned. We study the simplest example of biaxial molecular arrangement, namely, the disclination defect of strength +1 corresponding to a uniform, cylindrically symmetric, splay deformation of the director far from the core. This is imposed by choosing homeotropic anchoring conditions at the cylinder pore walls.

We take care to check the equilibration of our simulations, and note that quite extensive runs are required to ensure this. We also study in particular the effects of pore size, with radius varying from 2 to 5 times the molecular length, so as to eliminate the effects of the walls on the defect core. More precisely, our aim is to restrict these effects to those that arise from the planar radial far-field structure, rather than from density and order-parameter variations in the immediate vicinity of the walls. It is well known that the pore radius

plays a critical role in determining the stability of different nematic structures in this geometry. An analysis of the elastic free energy shows that the ''escaped radial'' structure, in which the director bends over to become parallel with the symmetry axis in the core region, is the stable structure for large pore radius [19,20]. In analyzing experiments on nematic liquid crystals in cylindrical pores, Crawford *et al.* [21,22] show that at small pore radii, the escaped structure (which will also, in general, have point defects along the disclination line) is not the most stable; they discuss the planar radial and planar polar configurations, finding the latter to be stable for the parameter values that they survey.

A unified presentation of the different theories is given in Sec. II. The model, and simulation techniques, are set out in Sec. III. The observed structures are described in Sec. IV, along with theoretical fits to the order parameter profiles. A discussion of the results, and the validity of the theories, together with some concluding remarks, appear in Sec. V.

II. PHENOMENOLOGICAL MODELS

In the framework of the continuum theory, the system can be described by the Landau–de Gennes free-energy density [2]:

$$F=\kappa|\nabla\mathbf{Q}|^2+\sigma(\mathbf{Q}), \tag{1}$$

where $\sigma(\mathbf{Q})$ is a function of the invariants of $\mathbf{Q}$, the symmetric order tensor. This is the suitably normalized traceless part of the tensor $\mathbf{M}$ of the second moments of the molecular orientational distribution function f,

$$\mathbf{M}=\int f(\mathbf{u})\mathbf{u}\otimes\mathbf{u}d\Omega.$$

$$\mathbf{Q}=\tfrac{3}{2}\mathbf{M}-\tfrac{1}{2}\mathbf{I}, \tag{2}$$

where $\mathbf{I}$ is the unit tensor and the integration is over the unit sphere.

We exclude the escape of the director in the z direction, and our boundary conditions also prevent spiral configurations, so the eigenvectors of $\mathbf{Q}$ coincide with the unit vectors of the cylindrical geometry, namely, $\mathbf{e}_\rho$, $\mathbf{e}_\theta$, and $\mathbf{e}_z$, respectively, in the radial, tangential, and axial directions. Since the eigenvalues of $\mathbf{Q}$ are not independent, the tensor may be expressed in terms of two independent parameters: the order parameter S and biaxiality α [5]:

$$\begin{aligned}\mathbf{Q}&\equiv Q_{\rho\rho}\mathbf{e}_\rho\otimes\mathbf{e}_\rho+Q_{\theta\theta}\mathbf{e}_\theta\otimes\mathbf{e}_\theta+Q_{zz}\mathbf{e}_z\otimes\mathbf{e}_z\\&=S\mathbf{e}_\rho\otimes\mathbf{e}_\rho+(-\tfrac{1}{2}S+\tfrac{3}{2}\alpha)\mathbf{e}_\theta\otimes\mathbf{e}_\theta+(-\tfrac{1}{2}S-\tfrac{3}{2}\alpha)\mathbf{e}_z\otimes\mathbf{e}_z.\end{aligned} \tag{3}$$

Minimizing the full free-energy functional (1) with respect to the S, α and taking into account that $S=S(\rho)$, $\alpha=\alpha(\rho)$, where ρ is the distance from the cylinder axis, we obtain the following Euler-Lagrange equations:

$$\begin{aligned}(\rho S')'-3\rho^{-1}(S-\alpha)-3g_1(S,\alpha)=0,\\(\rho\alpha')'+\rho^{-1}(S-\alpha)-g_2(S,\alpha)=0.\end{aligned} \tag{4}$$

Here $g_1(S,\alpha)=\frac{2}{9}\kappa^{-1}\partial\sigma/\partial S$, $g_2(S,\alpha)=\frac{2}{9}\kappa^{-1}\partial\sigma/\partial\alpha$, and the prime denotes differentiation with respect to ρ.

The system of equations (4) should be solved with corresponding boundary conditions. The boundary conditions at $\rho=0$ can be obtained if we look for the solutions close to the center of the disclination line. Indeed, in the limit $\rho\to0$, we can neglect the functions g_1,g_2 in Eqs. (4). Then, seeking the solution as an expansion in powers of ρ, one can obtain that in the region close to the center of the disclination line the solutions are

$$S=S_0+3\gamma\rho^2,\quad \alpha=S_0-\gamma\rho^2, \tag{5}$$

where S_0 and γ are constants. Therefore, at $\rho=0$, we have

$$S'|_{\rho=0}=0,\quad \alpha'|_{\rho=0}=0. \tag{6}$$

We also assume that, far away from the disclination core, we have a uniaxial nematic, and the surface at $\rho=R$ provides the order parameter S_s:

$$S|_{\rho=R}=S_s,\quad \alpha|_{\rho=R}=0. \tag{7}$$

Some general properties of Eqs. (4), regardless of the explicit form of the functions g_1,g_2, can help us to fit the simulation results. The simulations provide the value of the order parameter on the disclination line S_0, which we can also derive analytically. Indeed, the solutions (5) imply that $S+3\alpha|_{\rho\to0}=\text{const}$. The condition that the energy is bounded requires also $S_0=\alpha_0$. Therefore, from Eq. (4) we obtain the implicit equation for the order-parameter value on the disclination line

$$g_1(S_0,S_0)+g_2(S_0,S_0)=0. \tag{8}$$

Now we consider the particular models.

A. Full free-energy expansion

A widely used formula for σ is Landau–de Gennes':

$$\sigma_{\mathrm{LG}}=a\,\mathrm{Tr}\,\mathbf{Q}^2-b\,\mathrm{Tr}\,\mathbf{Q}^3+c[\mathrm{Tr}\,\mathbf{Q}^2]^2, \tag{9}$$

where a is assumed to depend linearly on the temperature, whereas positive constants b,c are considered temperature independent. For this free energy, the *uniaxial nematic* state is stable when $b^2>24ca$ with the degree of orientational ordering

$$S_b=\frac{b}{8c}\left(1+\sqrt{1-\frac{64ca}{3b^2}}\right). \tag{10}$$

Taking into account the parametrization (3), the suitably rescaled potential (9) may therefore be rewritten as

$$\begin{aligned}\sigma_{\mathrm{LG}}=k\{&S^2(\tfrac{1}{2}S^2-\tfrac{2}{3}S(S_b+S_u)+S_bS_u)\\&+\alpha^2[3S_uS_b+6(S_u+S_b)S+3S^2+\tfrac{9}{2}\alpha^2]\},\end{aligned} \tag{11}$$

so that the turning points for the uniaxial nematic phase with $\alpha=0$ occur at $S=S_u,S_b$.

The functions g_1, g_2 then read

$$\lambda^2 g_1 = S_u S_b S + (S_u + S_b)\{3\alpha^2 - S^2\} + S\{3\alpha^2 + S^2\},$$
$$\lambda^2 g_2 = 3 S_u S_b \alpha + 6(S_u + S_b) S\alpha + 3\alpha\{3\alpha^2 + S^2\}, \tag{12}$$

where $\lambda^2 = \frac{9}{4}\kappa/k$ is the characteristic length. Equation (8) provides us with the values of the order parameter and biaxiality on the disclination line:

$$S_0 = \alpha_0 = -\tfrac{1}{2} S_u . \tag{13}$$

B. Biscari and Virga approach

In order to obtain analytical expressions for the order parameter profile, Biscari and Virga [5] used a quadratic approximation to the full free energy σ, expressed in terms of S and α,

$$\sigma_{\mathrm{BV}} = k\{\eta(S - S_b)^2 + \alpha^2\}, \tag{14}$$

with the following expressions for the functions g_1, g_2:

$$g_1 = \frac{\eta}{\lambda^2}(S - S_b), \quad g_2 = \frac{1}{\lambda^2}\alpha.$$

The order parameter at the center of the disclination line then reads

$$S_0 = \frac{\eta}{1+\eta} S_b . \tag{15}$$

C. Mottram and Hogan approach

Another model, considered by Mottram and Hogan [6] uses a quartic potential in S but retains a quadratic potential in α

$$\sigma_{\mathrm{MH}} = k\{\eta S^2[\tfrac{1}{2}S^2 - \tfrac{2}{3}S(S_b + S_u) + S_b S_u] + \alpha^2\}. \tag{16}$$

This potential provides the following functions g_1, g_2:

$$g_1 = \frac{\eta}{\lambda^2} S(S - S_u)(S - S_b), \quad g_2 = \frac{1}{\lambda^2}\alpha,$$

and the following value of the order parameter on the disclination line:

$$S_0 = \tfrac{1}{2}\{S_u + S_b \pm \sqrt{(S_u - S_b)^2 - 4\eta^{-1}}\}. \tag{17}$$

D. Maier-Saupe approach

Another mean-field approach to the description of the disclination line was considered by Sigillo *et al.* [7]. They applied Maier-Saupe theory and obtained expressions for the functions g_1, g_2. The Maier-Saupe theory has an intermolecular potential strength U as the only adjustable parameter, determining the correct value of the bulk order parameter $S_b(U)$. The value of the order parameter S_0 on the disclination line is then fixed and determined by the value of S_b.

III. MOLECULAR MODEL AND SIMULATION METHODS

The molecules in this study are modeled as hard ellipsoids of revolution of elongation $e = A/B = 15$, where A is the length of the major axis and B the length of the two equal minor axes. The phase diagram and properties of this family of models are well studied [23–26,10]. Units of length are chosen such that $AB^2 = 1$, making the molecular volume equal to that of a sphere of unit diameter. It is useful to express the density as a fraction of the close-packed density for perfectly aligned hard ellipsoids, assuming an affinely transformed face-centered-cubic or hexagonal-close-packed lattice; in reduced units $\varrho^*_{\mathrm{cp}} = \varrho_{\mathrm{cp}} AB^2 = \sqrt{2}$. Henceforth, the asterisks denoting reduced quantities will be omitted.

The molecules were confined within a cylinder of radius R, and height H, with periodic boundary conditions applied in the z direction (the symmetry axis). The cylindrical confining walls are defined by the condition that they cannot be penetrated by the *centers* of the ellipsoidal molecules. Packing considerations generate *homeotropic* ordering at the surface, i.e., the molecules prefer to orient themselves normal to the interface, without the need to apply an explicit ordering field. The properties of such surfaces in planar geometry were investigated previously [16]. For these particles, the isotropic-nematic phase transition occurs at quite low density, $\varrho/\varrho_{\mathrm{cp}} \approx 0.2$. Temperature is not a significant thermodynamic quantity in this model; we set $k_B T = 1$ throughout.

Monte Carlo simulations were carried out for systems of the following cylinder radii: $R/A = 2.08$, 2.67, 4.00, 5.33. The corresponding numbers of ellipsoids were $N = 3500$, 6000, 13 000, 22 000. The height H/A was in the range 2.6–2.8 in all cases. All the simulations were conducted at the same state point used in the earlier study [16], corresponding to a bulk pressure $P = 2.0$ in the above reduced units; this is significantly higher than the isotropic-nematic coexistence pressure $P \approx 1.49$ [27]. No external fields were applied, and conventional Monte Carlo moves were employed, with translational and rotational displacements chosen to give a reasonable acceptance rate.

The simulation results were analyzed to give a density profile, averaged over cylindrical shells of width $0.125B - 0.25B$, and an order tensor profile obtained by averaging

$$Q_{\alpha\beta}(\rho_i) = \left\langle \frac{1}{n_i} \sum_{j=1}^{n_i} \left\{ \frac{3}{2} u_{j\alpha} u_{j\beta} - \frac{1}{2}\delta_{\alpha\beta} \right\} \right\rangle, \quad \alpha, \beta = \rho, \theta, z,$$

where there are n_i molecules present in bin i; $\delta_{\alpha\beta}$ is the Kronecker delta. The axis system is resolved as before into radial (ρ), tangential (θ), and axial (z) components, for the purposes of accumulating these functions. Therefore, the tensor components $Q_{\alpha\beta}$ have been averaged over global rotations of the system (positions and orientations together) about the symmetry axis, as well as global translations in the z direction. Diagonalizing this tensor, for each bin, gives three eigenvalues and three corresponding eigenvectors. This procedure allows us to test for (a) the planar radial structure, for which the eigenvectors lie along the ρ, θ, z coordinate axes, independent of ρ, and the eigenvalues are $Q_{\rho\rho}(\rho)$, $Q_{\theta\theta}(\rho)$, $Q_{zz}(\rho)$, and (b) the escaped radial structure, for which one of the eigenvectors points along the θ direction

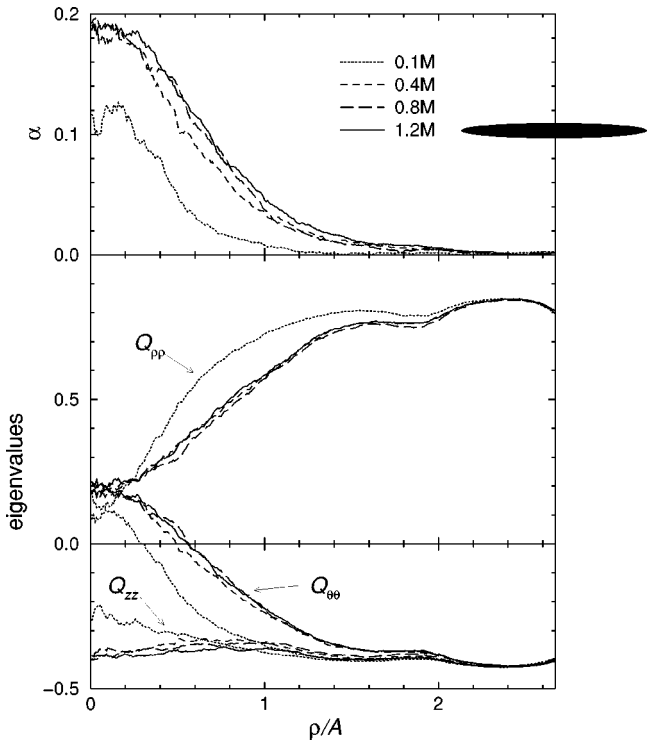

FIG. 1. Time evolution of a system started from a perfect planar radial configuration, in a cylinder of radius $R/A=2.67$. We show order-tensor eigenvalue profiles averaged over 10^5 sweeps, taken at the indicated times (units of 10^6 sweeps). The top eigenvalue is $Q_{\rho\rho}$, the middle one $Q_{\theta\theta}$, and the bottom one Q_{zz} in each case. In the upper panel we plot the biaxiality parameter $\alpha=\frac{1}{3}(Q_{\theta\theta}-Q_{zz})$. Note that the biaxial core develops quite rapidly and that equilibration is essentially complete between 0.4 and 0.8×10^6 sweeps. The final equilibrium configuration is identical to that obtained from a disordered starting configuration. The shaded ellipse indicates the outermost, homeotropically anchored, layer at the cylinder wall.

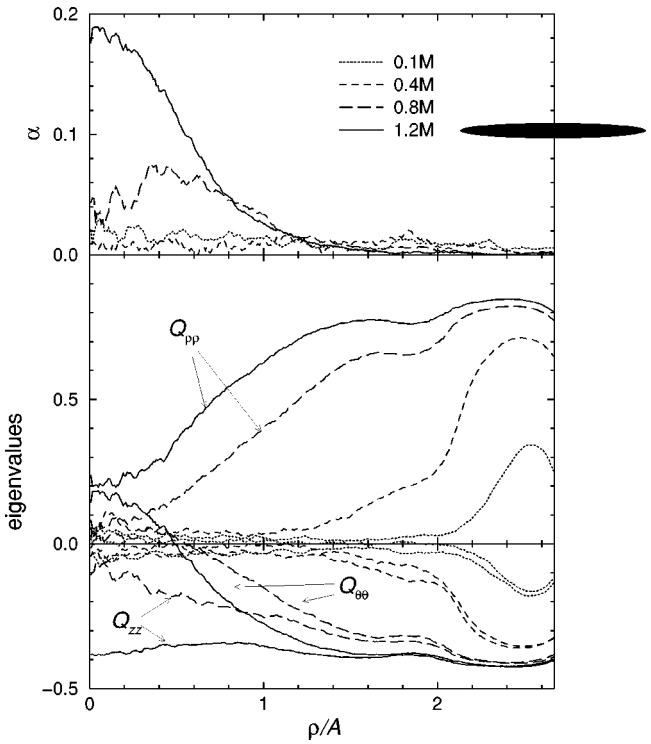

FIG. 2. Time evolution of a system started from an orientationally disordered configuration, in a cylinder of radius $R/A=2.67$. Notation as in Fig. 1. Note that the ordering remains uniaxial at the boundary and propagates in towards the center; as the ordering reaches the center, the biaxial disclination core develops. The final equilibrium configuration is identical to that obtained from a planar radial starting configuration.

for all values of ρ, and the other two lie in the ρ, z plane, changing their orientation as ρ varies.

The above tensor is not sensitive to any breaking of axial symmetry: instead, it gives a cylindrical average. To give a full representation of the positional variation of the orientational order, we must retain the full spatial dependence of **Q**. We find it convenient to calculate

$$S_{\alpha\beta}(\mathbf{r})=\frac{1}{n_{\mathcal{R}}}\sum_{j\in\mathcal{R}}u_{j\alpha}u_{j\beta}\quad\alpha,\beta=x,y,z, \tag{18}$$

where the sum is conducted over the $n_{\mathcal{R}}$ molecules found to be in a neighborhood $\mathcal{R}$ of the chosen point **r**. The eigenvectors of this **S** tensor are the same as those of the corresponding **Q**; the eigenvalues are linearly related and are nonnegative, so the tensor may be visually represented as a spheroid, whose principal axis directions and lengths are given by the eigenvectors and corresponding eigenvalues [28]. Then, a well ordered uniaxial region appears as an elongated, prolate shape; the uniaxial core of a disclination defect of strength $+1$ would appear as an oblate spheroid with its symmetry axis along the axis of the cylinder; disordered regions would correspond to a spherical shape, and so on.

IV. SIMULATION RESULTS

Most results were obtained from starting configurations in which the ellipsoids were positioned randomly, avoiding overlaps, but were perfectly aligned in the planar radial configuration. Typical equilibration times for these systems were around 7×10^5 MC sweeps (one sweep is one attempted move per particle), and this was monitored through the orientation profiles defined above. The development of a biaxial core in the system with $R/A=2.67$ is shown in Fig. 1; the other systems evolved in a similar way. Following equilibration, production runs of approximately 5×10^5 MC sweeps were undertaken.

Checks for convergence were carried out, starting from configurations in which molecular orientations as well as positions were disordered. The time evolution of the $R/A=2.67$ system is shown in Fig. 2. Note that the ordering remains uniaxial at the boundary, and propagates in towards the center; as the ordering reaches the center, the biaxial disclination core develops. An equilibration period of 10^6 sweeps was needed to reach the equilibrium planar radial structure, and a subsequent production run of 2×10^5 sweeps yielded results identical to those obtained from the planar radial starting point. For the larger cylinder radii, similar behavior was observed, but the time scale for propagation of the order from the boundary to the center was correspondingly longer. In each case, a run was conducted which was of sufficient length to confirm that the correct structure was becoming established.

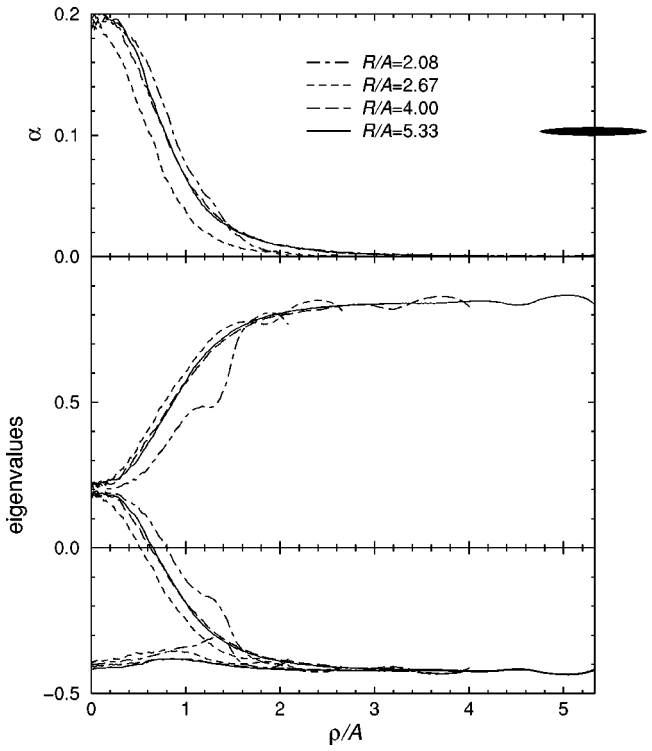

FIG. 3. Equilibrium order-tensor eigenvalue profiles for cylinders of indicated radii. For the two smallest cylinders, the walls clearly have an effect on the defect core structure; the results for the two largest cylinders are essentially indistinguishable. Notation as in Fig. 1.

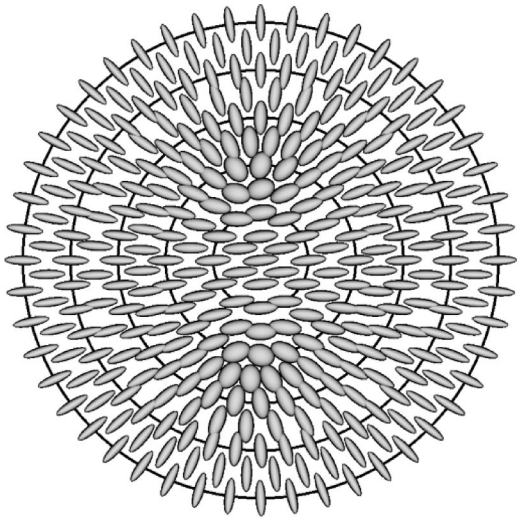

FIG. 4. Distribution of order tensor in the plane perpendicular to the cylinder axis, in the core region, for the case $R/A=4.00$. Concentric circles at half-integer intervals of radius ρ/A are plotted as a guide. The spheroid sizes are not physically significant. The figure is oriented so that the $+\frac{1}{2}$ defects lie above and below the cylinder axis.

In no case was the escaped radial structure formed during these runs. We have carried out some preliminary tests, for the pores of smaller radius, $R/A=2.08$, 2.67, in which the escaped radial structure was stabilized by the application of a uniform orienting field favoring alignment along the cylinder axis. Following removal of this field, the planar structure was seen to be recovered on a simulation time scale of 5×10^5 sweeps. Thus, the planar structure is thermodynamically stable for these cases, and it appears to be at least metastable on the time scales of our simulations for the larger pores.

In Fig. 3 the order-parameter profiles are presented for all the different cylinder sizes. The biaxiality profile $\alpha(\rho)=\frac{1}{3}(Q_{\theta\theta}-Q_{zz})$ indicates the extent of the core region. For the two smallest cylinders, it is clear that the walls act to deform the disclination core. For $R/A=2.08$, the core region is enlarged, while for $R/A=2.67$ it is compressed. The results for the two largest cylinders are almost indistinguishable.

In Fig. 4 we show the order tensor variation in the xy plane (no variation with z coordinate was observed) for the core region in the $R/A=4.00$ case. The **S**-tensor spheroid of Eq. (18) is plotted at a number of points (x_s,y_s) which lie on circles centered on the cylinder axis, separated by $0.25A$, with the neighborhood $\mathcal{R}$ of each point defined to include all molecules whose centers (x,y,z) satisfy $\sqrt{(x-x_s)^2+(y-y_s)^2}<0.25A$. The tensors are averaged over a run of 10^5 sweeps. The figure indicates that the core is actually best described as a pair of disclinations each of strength $+1/2$, symmetrically arranged at $\rho/A\approx1-1.25$ from the cylinder axis. Very similar results are seen for all the three largest pores, $R/A=2.67$, 4.00, 5.33, while for the smallest pore, $R/A=2.08$, the defects are slightly further out, at $\rho/A\approx1.5$. There is a small region of almost unperturbed uniaxial nematic liquid crystal around $\rho\approx0$, with the director perpendicular to the cylinder axis. We note that similar defect pairs are seen in the two-dimensional simulations reported in Ref. [18].

The order-tensor profiles reported in Fig. 3 are properly regarded as axial averages of structures which are not themselves axially symmetric on the time scales of the simulation. This is why the lowest eigenvalue in the profiles of Fig. 3 adopts similar values inside and outside the core: it corresponds to the eigenvector along the cylinder axis, and is unaffected by the axial averaging. We discuss in Sec. V the validity of carrying out such an axial average, simply noting here that it is the most straightforward way of comparing our simulation results with theories that assume cylindrical symmetry.

We have fitted the results for $R/A=4.00$ using the phenomenological theories of Sec. II. In each case, the boundary-value problem of Eqs. (4), (6), (7), was solved using the relaxation method [29]. In Figs. 5, 6, the fitting curves and the original simulation data are shown. Note, that to fit the simulation data we first determined the value of the parameter η or S_u using Eqs. (13), (15), (17). Then we performed suitable rescaling, changing the factor λ.

V. DISCUSSION

One can see in Figs. 5 and 6 that the slope of the fitting curves in general reflects the structure of the core: the center of the core is strongly biaxial, extending over a few units of length, as shown by the splitting of the eigenvalues $Q_{\theta\theta}$, Q_{zz}, and hence the nonzero biaxiality parameter $\alpha(\rho)$. At the same time, the difference between the descriptions is also evident. Biscari and Virga's theory gives an incorrect shape

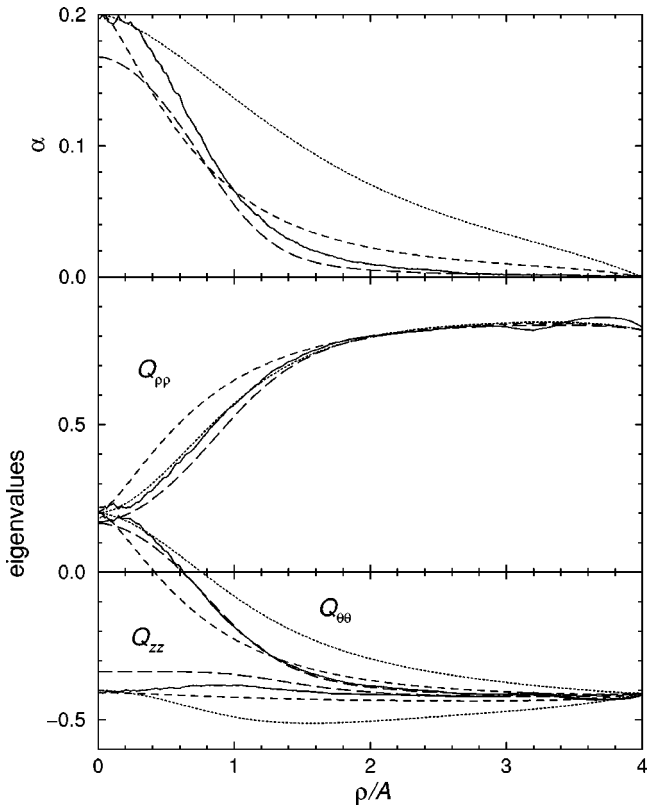

FIG. 5. Fits of simulation results (solid lines) to theoretical predictions discussed in the text. The best fit in each case was obtained for the following parameters: Mottram, Hogan [6] (dotted lines): Eq. (16), with $\eta/\lambda^2=1.58$, $\lambda^{-2}=1$, $R=6.5$, $S_b=0.88$, $S_s=0.82$, $S_u=0.01$. Biscari, Virga [5] (dashed lines): Eq. (14), with $\eta/\lambda^2=1$, $\lambda^{-2}=3.4$, $R=6$, $S_b=0.88$, $S_s=0.82$. Sigillo, Greco, Marrucci [7] (long dashed lines): $U=13$, $S_s=0.82$, $R=7$. Notation as in Fig. 1.

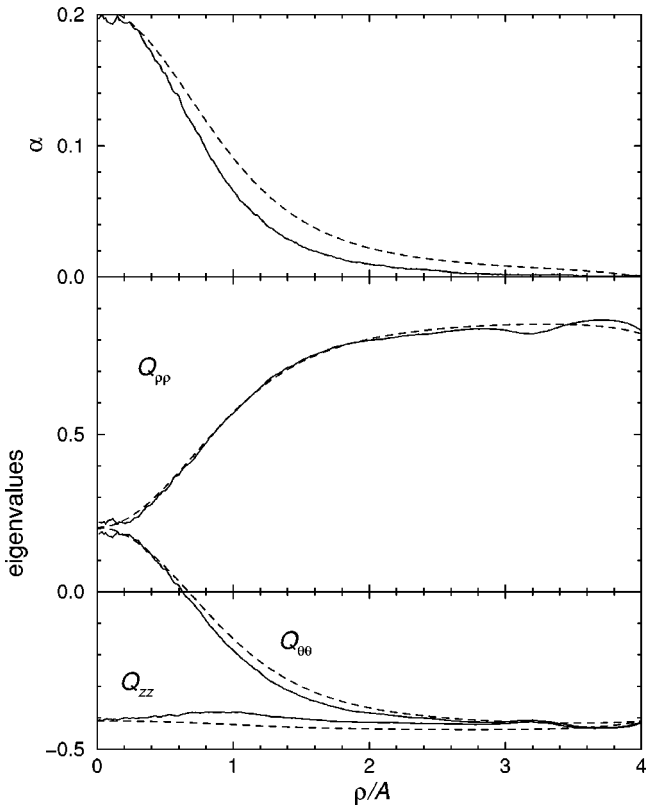

FIG. 6. Fit of simulation results (solid lines) to the Landau–de Gennes free-energy expansion (11) using the approach of Schopohl and Sluckin [3,4] (dashed lines). The best fit in each case was obtained for $\lambda^{-2}=1.42$, $R=6$, $S_b=0.88$, $S_s=0.82$, $S_u=-0.4$. Notation as in Fig. 1.

of $S(\rho)$ for small values of S (and hence small values of ρ here). This is fairly predictable, since a quadratic expansion of the free-energy density $F\sim\eta(S-S_b)^2$ was used, which is valid only for small deviations of the order parameter from the *bulk* value S_b.

The more sophisticated form of the free energy used by Mottram and Hogan (up to fourth order in S) corrects the slope of the curve for the order parameter $S=Q_{\rho\rho}$. However, the biaxial part $Q_{\theta\theta}-Q_{zz}$, still has only qualitative agreement with the simulation results, which is probably because of the *quadratic* approximation to the biaxial part of the free energy. This is particularly apparent in the $\alpha(\rho)$ profile, in which the biaxiality extends far beyond the core radius which would be deduced from $Q_{\rho\rho}$.

In spite of having only one adjustable parameter, the Maier-Saupe theory of Sigillo *et al.* gives a very realistic description of the disclination core structure. However, it predicts slightly lower core biaxiality than that obtained in the simulations.

The most accurate fitting we obtained used the full expansion of the free energy in powers of the order-parameter tensor (9), as shown in Fig. 6. This form, originally used by Schopohl and Sluckin, manages to reproduce the overall extent of the biaxial region quite well, while fitting the limiting behavior of both $\alpha(\rho)$ and $S(\rho)$ as $\rho\rightarrow 0$, and the magnitude of S in the bulk. Therefore, we can conclude that all the terms in the free-energy expansion (or at least up to the fourth order in the order-parameter tensor) should be taken into account if one wants to make the correct *quantitative* description of the disclination core structure.

Figure 4 shows that the core structure seen on the simulation time scale is not, in fact, cylindrically symmetrical, and this raises questions regarding the validity of averaging the order tensor over rotations about the cylinder axis. Such averaging may arise in a natural way. We see a small amount of rotation of the defect pair around the axis, of the order of 10°–15°, as the core structure evolves in time, during the 5×10^5-sweep simulation runs conducted here. If we roughly equate this to a real-time period of the order of nanoseconds, it seems possible that significant rotation will occur on the experimental time scale. The situation is further complicated when one considers correlations along the z direction; the periodic box employed here is quite small, but use of a much longer cylindrical pore might reveal some twisting of the separate $+\frac{1}{2}$ defect lines about the cylinder axis. Both effects would result in the kind of cylindrical averaging which we have carried out, but we can currently only speculate on this.

A second question concerns the distance between the $+\frac{1}{2}$ defect lines. We do not observe separation of the defect pair, either as the simulations proceed in time or as we study larger pores. Nonetheless, it is quite possible that the pore walls are confining the defect pair to the vicinity of the axis, and that they might separate if a much larger system were simulated. We note that, if they were to completely separate

and approach the pore walls, the result would be the planar polar structure discussed elsewhere [21,22]. It would be interesting to calculate free energies as a function of the defect separation to investigate this.

Finally, we may expect the escaped radial structure to become increasingly favored as the pore radius increases; it is clearly not the most stable structure for the smallest pores studied here. Once more, free-energy calculations are needed to make a proper comparison. Further work on these aspects is in progress.

ACKNOWLEDGMENTS

The advice of Nigel Mottram is gratefully acknowledged. This research was supported by EPSRC, and by the University of Bristol Department of Physics. D.A. also acknowledges support through Grant No. PSU082002 of the International Soros Science Education Program and Grant No. ORS/99007015 of the Overseas Research Students Award. The authors of Ref. [18] are thanked for providing a preprint of their paper.

[1] F. C. Frank, Discuss. Faraday Soc. **25**, 19 (1958).
[2] P. G. de Gennes and J. Prost, *The Physics of Liquid Crystals*, 2nd ed. (Clarendon Press, Oxford, 1995).
[3] N. Schopohl and T. J. Sluckin, Phys. Rev. Lett. **59**, 2582 (1987).
[4] N. Schopohl, Phys. Rev. Lett. **60**, 755(E) (1988).
[5] P. Biscari and E. G. Virga, Int. J. Nonlinear Mech. **32**, 337 (1997).
[6] N. J. Mottram and S. J. Hogan, Philos. Trans. R. Soc. London, Ser. A **355**, 2045 (1997).
[7] I. Sigillo, F. Greco, and G. Marrucci, Liq. Cryst. **24**, 419 (1998).
[8] M. P. Allen and D. Frenkel, Phys. Rev. A **37**, 1813 (1988).
[9] M. P. Allen and D. Frenkel, Phys. Rev. A **42**, 3641(E) (1990).
[10] B. Tjipto-Margo, G. T. Evans, M. P. Allen, and D. Frenkel, J. Phys. Chem. **96**, 3942 (1992).
[11] M. P. Allen *et al.*, J. Chem. Phys. **105**, 2850 (1996).
[12] J. Stelzer, L. Longa, and H.-R. Trebin, J. Chem. Phys. **103**, 3098 (1995).
[13] J. Stelzer, L. Longa, and H.-R. Trebin, Mol. Cryst. Liq. Cryst. **262**, 455 (1995).
[14] J. Stelzer, H.-R. Trebin, and L. Longa, J. Chem. Phys. **107**, 1295(E) (1997).
[15] J. Stelzer, L. Longa, and H.-R. Trebin, Phys. Rev. E **55**, 7085 (1997).
[16] M. P. Allen, Mol. Phys. **96**, 1391 (1999).
[17] S. D. Hudson and R. G. Larson, Phys. Rev. Lett. **70**, 2916 (1993).
[18] J. Dzubiella, M. Schmidt, and H. Löwen (unpublished).
[19] P. E. Cladis and M. Kléman, J. Phys. (Paris) **33**, 591 (1972).
[20] M. Kléman, *Points, Lines and Walls in Liquid Crystals, Magnetic Systems and Various Ordered Media* (Wiley, Chichester, 1983).
[21] G. P. Crawford *et al.*, Phys. Rev. A **44**, 2570 (1991).
[22] G. P. Crawford, D. W. Allender, and J. W. Doane, Phys. Rev. A **45**, 8693 (1992).
[23] D. Frenkel, B. M. Mulder, and J. P. McTague, Phys. Rev. Lett. **52**, 287 (1984).
[24] D. Frenkel and B. M. Mulder, Mol. Phys. **55**, 1171 (1985).
[25] M. P. Allen, Philos. Trans. R. Soc. London, Ser. A **344**, 323 (1993).
[26] M. P. Allen, G. T. Evans, D. Frenkel, and B. Mulder, Adv. Chem. Phys. **86**, 1 (1993).
[27] P. J. Camp *et al.*, J. Chem. Phys. **105**, 2837 (1996).
[28] M. P. Allen, Mol. Simul. **2**, 301 (1989).
[29] W. H. Press, B. P. Flannery, S. A. Teukolsky, and W. T. Vetterling, *Numerical Recipes in Fortran*, 2nd ed. (Cambridge University Press, Cambridge, 1992).